The Timing of High Sea Levels Over the Past 200,000 Years

Christina D. Gallup; R. Lawrence Edwards; Robert G. Johnson

Science, New Series, Vol. 263, No. 5148 (Feb. 11, 1994), 796-800.

The Timing of High Sea Levels Over the Past 200,000 Years

Christina D. Gallup, R. Lawrence Edwards, Robert G. Johnson

The ^{230}Th ages and $^{234}U/^{238}U$ ratios were determined for Barbados corals that grew during periods of high sea level within the last 200,000 years. The similarity of the initial $^{234}U/^{238}U$ ratios of some of the corals to the modern marine value suggests that these samples are pristine and that the marine $^{234}U/^{238}U$ ratio 83,000 and 200,000 years ago was within 2 per mil of the modern value. The accuracies of the ^{230}Th ages are evaluated on the basis of the $^{234}U/^{238}U$ values and a model of the behavior of uranium and thorium isotopes during diagenesis. For the last three interglacial and two intervening interstadial periods, sea level peaked at or after peaks in summer insolation in the Northern Hemisphere. This overall pattern supports the idea that glacial-interglacial cycles are caused by changes in Earth's orbital geometry. The sea-level drop at the end of the penultimate interglacial, the last interglacial, and a subsequent interstadial period lagged behind the decrease in insolation by 5,000 to 10,000 years.

Quaternary sea levels have fluctuated with the growth and decay of continental glaciers. Fossil corals record Quaternary sea levels and thus, when dated accurately, provide a test of the Milankovitch theory's predictions for the timing of the glacial cycles. This theory maintains that the variations in caloric summer solar insolation (that is, the solar radiation received at the top of the atmosphere that contributes to heating) at 65°N latitude modulate the glacial cycles (*1, 2*). The changes in insolation are driven by cyclical variations in the eccentricity of Earth's orbit and the tilt and precession of Earth's axis. To provide a rigorous test of the theory, one must determine the chronology of the sea-level record to within about ±2000 years, a value that provides sufficient resolution compared with the roughly 10,000-year interval between highs and lows in the intensity of 65°N summer insolation (*3*). Historically there have been a number of difficulties in dating fossil corals with this resolution.

The problem of dating imprecision was solved with the development of thermal-ionization mass-spectrometric (TIMS) techniques for measuring ^{230}Th (*4, 5*) and ^{234}U (*4–6*). However, inaccurate ages can result from diagenetic remobilization of uranium or thorium. We present data from coral terraces on Barbados that record high sea levels during the last interstadial and penultimate interglacial periods and at the end of the last interglacial period. We address the problem of diagenesis with a model that reproduces diagenetic trends in these and earlier uranium and thorium isotopic data and provides a criterion for distinguishing between accurate and inaccurate ages. Applying this criterion to new and previously reported data, we determined a record of high sea levels, which we compare to variations in 65°N summer insolation.

Minnesota Isotope Laboratory, Department of Geology and Geophysics, University of Minnesota, Minneapolis, MN 55455, USA.

We collected samples from coral terraces along two transects in Barbados, West Indies (Fig. 1): one on the Clermont Nose anticline (*7*) and the other on Holders Hill. The penultimate interglacial samples come from a remarkably well-preserved beach deposit at 91-m elevation in the Clermont Nose area. An overlying cemented surface appears to have protected both the coral cobbles and the unconsolidated carbonate sand in the deposit from extensive infiltration by ground water.

Uranium and thorium isotopic compositions and concentrations were determined by TIMS techniques. Most procedures are modifications of those previously reported (*4–6*). All replicates of ^{230}Th ages and initial $\delta^{234}U$ (defined in Table 1) values agreed within error (except the $\delta^{234}U$ value for the third replicate of AFM-20, analysis C) (Table 1).

We established a modern marine $\delta^{234}U$ value of 149.7 ± 1.5 by averaging the initial $\delta^{234}U$ value of an *Acropora palmata* coral cobble that we collected on a modern Barbados beach with three values from modern samples from Papua New Guinea (*8*) (error is 2σ of the population). This value is consistent with the range of $\delta^{234}U$ values from direct measurements of seawater (*6*).

Three samples from key points in the sea-level record have concordant ^{234}U-^{238}U and ^{230}Th ages (with use of the above value for the initial marine $\delta^{234}U$ value) (Table 1): FS-3 from the Worthing Terrace gives an age for substage 5a of 83.3 ± 0.3 thousand years (ka), and WAN-B-2 and WAN-B-7, both cobbles from the ancient beach deposit, give ages for substage 7.1 of 200.1 ± 1.2 and 200.8 ± 1.0 ka, respectively. The samples that do not have concordant ages have initial $\delta^{234}U$ values that are greater than the modern marine value. These high values are consistent with earlier observations from Barbadian and Bahamian fossil corals (*4, 5, 9–15*).

The high initial $\delta^{234}U$ values could be the result either of temporal changes in the marine $\delta^{234}U$ value or of diagenetic processes. Simple models that consider the marine inputs and residence time for uranium (*16*) indicate that the marine $\delta^{234}U$ value should not vary by more than 20 per mil over 10^5 years (*5, 12, 17*). We therefore follow earlier workers (*4, 5, 9–15, 17–20*) in concluding that most if not all of the elevated values result from diagenetic reactions. Because no aragonitic coral sample from Barbados has ever been documented with an initial $\delta^{234}U$ value less than the modern value, we assume that the samples with the lowest values experienced the least alteration and provide the most accurate records of past marine $\delta^{234}U$ values. We thus conclude that samples FSL-3, WAN-B-2, and WAN-B-7 indicate that the marine $\delta^{234}U$ value was within error of today's value 83.3 and 200 ka. Our data are consistent with other data that suggest that the marine $\delta^{234}U$ value has not changed by large amounts during the last 200 ka (*5, 8, 12, 17, 20*).

The mechanism whereby diagenetic reactions shift $\delta^{234}U$ values remains unknown, although models have been suggested (*10, 12, 14, 18*). To date, there have

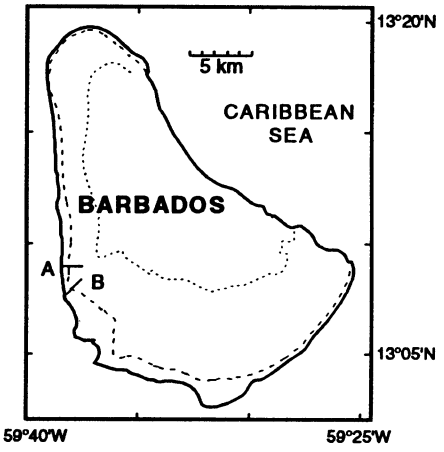

Fig. 1. Map of Barbados, West Indies, showing the first high cliff (dashed, the last-interglacial terrace), the second high cliff (dotted), the Holders Hill transect (A), and the Clermont Nose transect (B). Both transects are along major roadways: Clermont Nose is along the Gordon Cummins Highway, next to the University of the West Indies, and Holders Hill is along the road to the Bullen Agricultural Station from Highway 1. Sample elevations and terrace names are given in Table 1. Detailed sample locations are available from the authors upon request.

been no fossil coral data sets of sufficient size or precision to support any given model. Examination of our data in conjunction with earlier TIMS ^{230}Th Barbados data (Fig. 2) shows that for a given terrace or deposit, the samples with the highest initial δ^{234}U values appear to have the oldest ^{230}Th ages.

We generated a model to explain these trends and define a criterion for identifying samples that have inaccurate ^{230}Th ages. The rough trend between δ^{234}U value and ^{230}Th age can be explained by net addition of ^{234}U and ^{230}Th. We therefore assumed that ^{238}U concentration is constant, initial δ^{234}U value equals the modern marine value, and ^{234}U and ^{230}Th are continuously added during diagenesis. We determined an expression for the isotopic composition as a function of time for a coral that gains ^{234}U and ^{230}Th at constant rates from some outside source (*21*) and used the isotopic composition of an altered coral from Barbados to solve for rates of ^{234}U and ^{230}Th addition (*21*). We assumed that the ratio of the rate of ^{234}U addition to the rate of ^{230}Th addition is invariant and equal to the value calculated for this sample. We then calculated the possible isotopic compositions of materials of a given true age. These lie on an "addition line" (Fig. 2, dashed lines), the end point of which corresponds to the isotopic composition of material that experienced no diagenetic addition of ^{234}U or ^{230}Th. In general, one can calculate an addition line that is similar to the observed trend in the isotopic compositions of the material from a given terrace or deposit. The similarity between the modeled lines and the observed trends suggests that the true diagenetic processes affect both ^{234}U and ^{230}Th throughout the history of the coral (*21*).

The slopes of the addition lines (Fig. 2) allow us to estimate the difference between the ^{230}Th and true ages of a coral on the basis of the difference between the coral's initial δ^{234}U value and the modern marine δ^{234}U value. Because the data scatter about the modeled lines (*22*), we did not attempt to use the model to correct ^{230}Th ages of samples. Instead, we used the lines as a guide in establishing maximum acceptable initial δ^{234}U values. A sample with an initial δ^{234}U of 154, 4 δ-units above the marine value, has a ^{230}Th age about 1000 years older than its true age. Accordingly, for samples to have ^{230}Th ages accurate to within 2 ka, they should have an initial δ^{234}U value within 8 δ-units of the modern value.

We measured six fossil corals that have initial δ^{234}U values within 8 δ-units of the modern value: sample FS-3 (with a ^{230}Th age of 83.3 ± 0.3 ka), UWI-16 (117.0 ± 1.0 ka), UWI-2 (129.1 ± 0.8 ka) (*23*), WAN-B-1 (193.5 ± 2.8 ka), WAN-B-2 (200.1 ± 1.2 ka), and WAN-B-7 (200.8 ± 1.0 ka). The initial elevations of these samples record periods of relatively high sea levels (*24*) (Table 2). The 83.3- and 193.5-ka samples have initial elevations of −15.5

Table 1. Uranium and thorium isotopic composition and ^{230}Th ages of corals. The 2σ errors in the last significant figures are in parentheses.

Sample*	Elevation (m)	Deposit-Location§	^{238}U (ng/g)	^{232}Th‖ (pg/g)	δ^{234}U measured¶,#	[^{230}Th/^{238}U] activity**,#	Age** (ka)	δ^{234}U initial††,#
				Modern				
FSL-2	0	C-MB	3208 (3)	165 (3)	148.6 (1.6)	0.0014 (3)	0.132 (3)	148.7 (1.6)
				Interstadials				
FS-3	12	RC-W	3276 (2)	87 (13)	119.2 (1.2)	0.6059 (13)	83.3 (0.3)	151.0 (1.5)
FS-8	13	RC-W	3367 (2)	99 (12)	131.3 (1.2)	0.6323 (23)	87.2 (0.5)	168.1 (1.6)
FT-1	24	RC-V	3623 (2)	356 (18)	142.3 (1.2)	0.7165 (12)	104.3 (0.4)	191.3 (1.7)
				Last interglacial				
AFM-20 (A)	58	RC-RH	3233 (2)	383 (8)	113.5 (1.4)	0.7904 (18)	130.2 (0.7)	164.2 (2.1)
AFM-20 (B)			3233 (2)	392 (3)	112.3 (1.5)	0.7897 (19)	130.3 (0.7)	162.5 (2.2)
AFM-20 (C)			3228 (3)	368 (5)	117.7 (1.8)	0.7889 (18)	128.7 (0.7)	169.6 (2.6)
UWI-2	31	‡‡-RH	3163 (3)	162 (6)	109.3 (1.4)	0.7832 (24)	129.1 (0.8)	157.6 (2.1)
UWI-16	40	C-RH	3309 (2)	25 (25)	113.6 (1.2)	0.7452 (36)	117.0 (1.0)	158.3 (1.8)
FU-1	47	RC-RH	2989 (2)	31 (31)	113.0 (1.2)	0.7720 (52)	124.6 (0.5)	160.9 (1.7)
FU-3	40	RC-RH	3812 (2)	19 (19)	132.1 (1.3)	0.8237 (29)	135.4 (0.7)	193.8 (1.9)
				Penultimate interglacial				
WAN-B-2 (1)	92	C-BD	2955 (3)	245 (16)	83.7 (1.1)	0.9264 (18)	199.0 (1.3)	147.1 (2.0)
WAN-B-2 (2)		C-BD	3049 (2)	488 (14)	82.8 (1.3)	0.9242 (30)	201.2 (2.0)	146.5 (2.4)
WAN-B-7	91	C-BD	2565 (2)	105 (7)	86.2 (1.1)	0.9321 (12)	200.8 (1.0)	152.3 (2.0)
WAN-B-1	91	C-BD	3019 (2)	639 (6)	91.6 (2.0)	0.9250 (45)	193.5 (2.8)	158.6 (3.7)
WAN-B-6†	91	C-BD	2501 (2)	165 (4)	96.0 (2.2)	0.9470 (15)	203.6 (1.7)	171.0 (4.0)
WAN-B-8	91	C-BD	2958 (2)	280 (4)	101.4 (1.3)	0.9525 (17)	203.5 (1.3)	180.5 (2.4)
WAN-B-5	91	C-BD	2893 (2)	107 (25)	116.0 (1.3)	0.9989 (53)	223.3 (3.8)	218.5 (3.4)
WAN-B sand	91	C-BD	1157 (1)	52,700 (150)	126.4 (3.0)	1.076 (18)	279.9 (+21/−19)	279.4 (+19/−18)
WAN-B-14	92	C-BD	3107 (2)	84 (18)	102.2 (1.4)	0.9308 (18)	190.8 (0.7)	175.6 (2.1)
WAN-E-1	83	RC–D-CH	3134 (2)	117 (20)	99.6 (1.4)	0.9598 (23)	209.2 (1.7)	180.2 (2.7)
WAN-C-1‡	78	FR	3011 (4)	125 (20)	96.4 (1.3)	0.9471 (70)	203.4 (4.0)	171.7 (3.2)
				Older terraces				
FY-2	63	RC	3192 (2)	39 (24)	124.8 (1.2)	0.9896 (22)	211.0 (1.6)	226.9 (2.4)
WAN-D-3 (1)	69	RC	3088 (2)	627 (11)	97.7 (2.3)	0.9885 (41)	230.5 (+3.7/−3.6)	187.7 (4.8)
WAN-D-3 (2)			3042 (2)	126 (81)	100.8 (2.0)	0.9847 (71)	225.1 (+5.5/−5.3)	190.8 (+4.9/−4.8)
WAN-D-3 (3)			3060 (3)	211 (34)	101.1 (2.5)	0.9955 (91)	232.9 (+7.6/−7.2)	195.7 (+6.4/−6.2)
FW-1	64	RC	4623 (2)	45 (45)	188.0 (1.3)	1.1535 (36)	283.7 (4.2)	420.3 (5.8)
WAN-A-1	99	RC-T	3522 (2)	679 (25)	144.3 (1.7)	1.1159 (38)	302 (6.0)	340.0 (7.0)
WAN-F-4	100	RC-T	3748 (3)	102 (89)	169.2 (2.3)	1.2008 (25)	402 (+12/−11)	529.0 (+19/−18)

*Duplicates denoted (A), (B), and (C) are aliquots of the same sample; those denoted (1), (2), and (3) are fragments of the same hand specimen. Analyses of all three aliquots of AFM-20 match those made at the California Institute of Technology (*4*) on the same sample. The "F" sample names are from the Holders Hill transect; all others are from Clermont Nose. All samples are *A. palmata*, except as marked. †*Siderastria* sp. ‡*Porites* sp. §Samples are from cobble (C), reef crest (RC), or forereef (FR) deposits and are located either on the modern beach (MB), the Worthing (W), Ventnor (V), Rendezvous Hill (RH), Durants–Cave Hill (D-CH), or Thorpe (T) terraces, or in the ancient beach deposit (BD). ‖Corrected for the analytical blank of 0.02 ± 0.01 pmol of ^{232}Th (error predominantly from uncertainty in the blank correction). ¶$\delta^{234}U_{measured} = [(^{234}U/^{238}U)_{measured}/(^{234}U/^{238}U)_{eq} - 1] \times 10^3$, where $(^{234}U/^{238}U)_{eq}$ is the secular equilibrium atomic ratio: $\lambda_{238}/\lambda_{234} = 5.472 \times 10^{-5}$. #Values for decay constants (λ) are as in (*4, 5*). **$[^{230}Th/^{238}U]_{activity} - 1 = e^{-\lambda_{230}T} + (\delta^{234}U_{measured}/1000)[\lambda_{230}/(\lambda_{230} - \lambda_{234})](1 - e^{-(\lambda_{230}-\lambda_{234})T})$, where T is the age in years (*39*). ††$\delta^{234}U_{initial} = [\delta^{234}U_{measured}][e^{\lambda_{234}T}]$. ‡‡See (*23*).

± 2.5 m and 3 ± 6 m, respectively, and predate subsamples of a Bahamian speleothem [dated by TIMS ^{230}Th techniques (*25*)] that constrain sea level to lower than −17 m at 79.7 ± 1.8 ka and lower than −14 m at 190 ± 5 ka. Thus, it appears that sea level dropped from peak levels within a few millennia after each coral sample grew. The 117.0-ka sample is an *A. palmata* coral cobble from a sand-cobble deposit that stratigraphically overlies the last interglacial forereef; thus, it appears to record the sea-level regression after the last interglacial period. The youngest accurate TIMS age (on the basis of our model, see below) for the top of the last interglacial terrace is 120.2 ka (*15*), when sea level was 2 to 8 m above present levels (*10, 26*). Thus, the samples with ages of 117.0 and 120.2 ka suggest that the average rate of sea-level drop was 5.3 ± 2.2 mm/year after the last interglacial, consistent with earlier estimates from Bahamian corals (*10*).

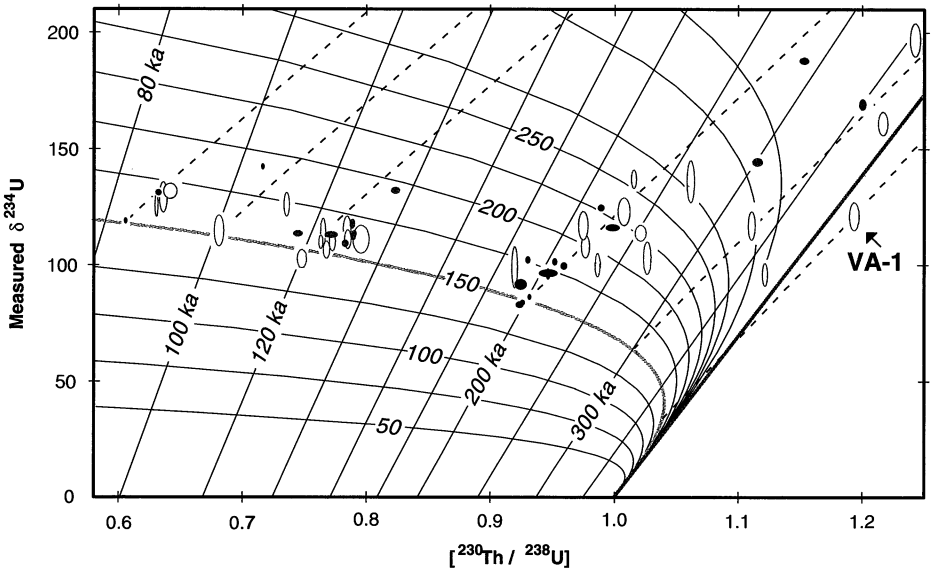

Fig. 2. Plot of measured $\delta^{234}U$ versus $^{230}Th/^{238}U$ activity ratio (*5*) with all TIMS Barbados data [this study and (*4, 5, 9, 12–15*)] for samples older than 80 ka. Each point is a 2σ error ellipse; solid ellipses are from this study. Data are grouped by generally increasing terrace elevation [nomenclature as in (*21, 38*)]: from left to right—Worthing Terrace (purple), Ventnor Terrace (blue), Rendezvous Hill Terrace (green), Kendall ill, Golden Grove, and Durants Terraces (purple, the next highest in elevation above the Rendezvous Hill Terrace), WAN-B, WAN-E, and WAN-C (blue), Thorpe, Kingsland-Aberdare, and Husbands terraces (green), Adam's Castle and St. Davids terraces (purple), and Hill View (VA-1, blue). The curved lines are contours of initial $\delta^{234}U$ value, and lines with steep positive slope are contours of ^{230}Th age. The contour for initial $\delta^{234}U$ = 150 (beige) corresponds to the modern marine $\delta^{234}U$ value. Data that plot along this contour have concordant ^{230}Th and $^{234}U/^{238}U$ ages. The area without contours to the right of the brown infinite ^{230}Th-age contour represents isotopic compositions that are inaccessible through closed-system decay. Dashed lines are ^{234}U-^{230}Th addition lines from our model (see text) calculated with ages of 83, 100, 120, 200, 300, and 520 ka. The similarity in the slope of the addition lines to the trend in the data by terrace suggests that the model reproduces, to a first approximation, the effects of diagenesis on the isotopic composition of Barbados corals. This allows us to estimate the effect of shifts in $\delta^{234}U$ on ^{230}Th age.

Because there is a range in analytical errors for previously published $\delta^{234}U$ values from Barbadian and Bahamian fossil corals (*4, 5, 9, 10, 12–15, 27, 28*), we applied our criterion to the nominal values (*29*) (Fig. 3A). Samples with ages that meet our criterion record sea levels that appear to correlate with oxygen isotope stages and substages 1, 5a, 5c, 5e, and 7.1 (Fig. 3).

All of the relatively high positions of sea level in the last 200 ka either coincide with or shortly postdate a relatively high 65°N summer insolation value (Fig. 3A and Table 2). This pattern is consistent with the idea that global climate is forced by orbital cycles. In the four cases where we have tight constraints on the timing of the drop in sea level from peak values (the last three interglacials, including the present, and the 83-ka high sea level), there is a significant phase lag between the time of insolation decrease and sea-level drop, from 5,000 ± 2,000 years to greater than 11,000 years. For all three interglacial periods, sea level

Table 2. The coral and speleothem sea-level records and their relation to the 65°N summer insolation (*3*). Also shown are the SPECMAP chronology for the deep-sea oxygen isotope record (*33*), a proxy for sea level, and the Devils Hole chronology for climate events recorded by oxygen isotope variations in Devils Hole calcite (*31*). For oxygen isotope stages and substages, the timing of peak values is given; for boundaries between oxygen isotope stages or substages, the timing of half-peak values is given.

Oxygen isotope stage	Past sea levels		Insolation and sea level			Other chronologies	
	Timing (ka)*	Elevation relative to present*,† (m)	Timing of 65°N summer insolation (ka)	Time difference between insolation peak and earliest high sea level‡ (ka)	Time difference between initial insolation drop and initial sea-level drop‡ (ka)	Devils Hole (ka)	SPECMAP (ka)
1	0 to 6	0	11	6	>11		2
1/2	11.5		18				11
4/5	79.7	<−17	78		5 ± 2	73	71
5a	83.3	−13 to −18	86	3 ± 1		80	80
5c	100.5	−12 to −17	103	3 ± 1		103	100
5d/5e	117	−11 to −17	122		10 ± 2	119	115
5e	120 to 130	2 to 8	128	−2 ± 2		122 to 132	122
5/6	>130		134.5			140	128
6/7	190	<−14	194		8^{+7}_{-4}	184	188
7.1	193 to 201	−6 to 9	200	−1 ± 2		196	194 to 196

*Values for stage 1 are from (*40*), values for stage 4/5 and 6/7 transitions are from speleothems (*25*), and values for other events are based on our data and references in text. †See (*24*). ‡Positive values indicate that the insolation peak preceded the sea-level event; negative values indicate that the sea-level event preceded the insolation peak.

remained high about 10,000 years or more after insolation began to decrease. Thus, large lag times appear to be a general characteristic of transitions from interglacial (or interstadial) to glacial periods.

There are also individual characteristics to each high sea level. Each has a different ratio of peak insolation to peak sea-level height. Furthermore, the earliest high sea level and peak insolation are almost coincident for the last and penultimate interglacials, but for the present interglacial, peak sea-level elevations were attained 5000 years after the insolation peak. The different character of each event suggests that the climatic response to orbital forcing is nonlinear (*30*), that global climate is influenced by factors in addition to orbital forcing (*31, 32*), or that the 65°N summer insolation curve is not the correct orbital forcing function.

In general, agreement for the timing of climatic events is excellent among the Devils Hole (*31*) and SPECMAP (*33*) oxygen isotope records and the coral and speleothem sea-level records (Fig. 3B), although the SPECMAP time scale for 5a and 5e appears to be offset to younger ages. This offset may indicate that, in detail, the assumptions used to tune the SPECMAP record may not faithfully mimic the true climatic response to orbital forcing.

The penultimate deglaciation has been proposed as a period when factors other than orbital forcing caused major changes in ice volume (*34*). Early ^{230}Th dating (by alpha counting) of Terrace VIIa in Papua New Guinea (*35*) suggested that sea level had reached high levels at about 140 ka, before the rise in 65°N summer insolation. If this were true, the penultimate deglaciation could not have been triggered directly by orbital forcing. Our analysis of the high-resolution data for the last interglacial period shows no evidence for high sea level before 130 ka (*28*). However, ^{230}Th dates of the Devils Hole calcite vein imply that the Earth was halfway through deglaciation at 140 ± 3 ka, or 5000 ± 3000 years before insolation reached half of its peak value (*31*) (Table 2 and Fig. 3B). Although the inferred age for deglaciation may prove to be valid, the record has a number of potential problems. The ages may be artificially high because of ^{230}Th incorporated during calcite growth (*36*). The oxygen isotope values represent regional climatic conditions, which may not be the same as global climatic conditions (*37*). Additionally, the value of 140 ± 3 ka was determined by interpolation between the closest directly dated subsamples (132 ± 3 and 150 ± 3 ka). Errors may be associated with the assumed constant growth rate over this 18,000-year period, which differs from the overall growth rate of the deposit. Further investigation into the timing of the penultimate deglaciation and of other key climatic events will be aided by continued application of TIMS techniques to the radiometric dating of carbonates, which may include the ^{235}U-^{231}Pa chronometer as a check for the accuracy of ^{230}Th ages.

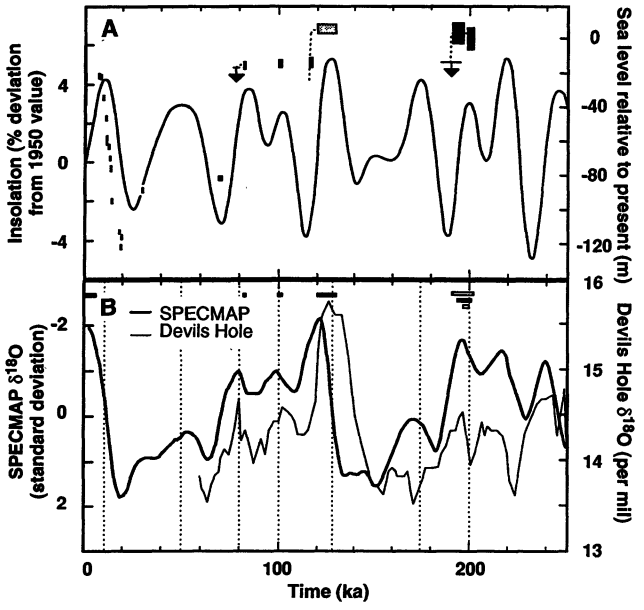

Fig. 3. (**A**) 65°N caloric summer solar insolation (*3*) (curve, left axis) and sea-level elevation (boxes, right axis) versus time. Boxes represent sea-level data from Barbadian and Bahamian corals that meet our criterion for accuracy, where dimensions correspond to errors in sea level and ^{230}Th age. Each solid box represents data from one Barbadian coral [this study, (*9, 27*); all samples are *A. palmata*; elevations have been corrected for tectonic uplift]. The stippled box represents the range of ages and elevations from five Barbadian [this study, (*4, 5, 9, 15*)] and 18 Bahamian samples (*10*) from the last interglacial period. Arrows represent maximum sea levels constrained by Bahamian speleothems (*25*), where the length of the horizontal line above each arrow represents the error in age for a subsample. Dashed lines are inferred sea-level changes. Sea level highs either coincide with or postdate a peak in insolation, and for the last three interglacials and the 83-ka high sea level, there are lags of 5 ± 2 to >11 ka between insolation decrease and sea-level drops. (**B**) The SPECMAP (*33*) and Devils Hole (*31*) oxygen isotope records versus time. Solid bars correspond to the time of high sea level as given by coral dates for the present, last, and penultimate interglacial periods and as given by single-coral analyses, including errors, for the 101- and 83-ka high-sea stands. The open bars represent the maximum and minimum duration of high sea level during the penultimate interglacial, estimated by the consideration of errors on coral ages. The dotted lines correspond to the peaks in 65°N summer insolation [from (A)]. In general, there is excellent agreement between the timing of the oxygen isotope records and the coral and speleothem records. The main discrepancies occur at about the time of the last interglacial period.

REFERENCES AND NOTES

1. M. M. Milankovitch, *Canon of Insolation and the Ice Age Problem* (Koniglich Serbische Akademie, Belgrade, Yugoslavia, 1941) (English translation, Israel Program for Scientific Translations, Washington, DC, 1969).
2. J. D. Hayes, J. Imbrie, N. J. Shackleton, *Science* **194**, 1121 (1976).
3. A. L. Berger, *Quat. Res.* **9**, 139 (1978), and tabulated values supplied by A. L. Berger.
4. R. L. Edwards, J. H. Chen, G. J. Wasserburg, *Earth Planet. Sci. Lett.* **81**, 175 (1987); R. L. Edwards, J. H. Chen, T.-L. Ku, G. J. Wasserburg, *Science* **236**, 1547 (1987).
5. R. L. Edwards, thesis, California Institute of Technology (1988).
6. J. H. Chen, R. L. Edwards, G. J. Wasserburg, *Earth Planet. Sci. Lett.* **80**, 241 (1986).
7. F. W. Taylor and P. Mann, *Geology* **19**, 103 (1991).
8. R. L. Edwards *et al.*, *Science* **260**, 962 (1993).
9. E. Bard, B. Hamelin, R. G. Fairbanks, *Nature* **346**, 456 (1990).
10. J. H. Chen, H. A. Curran, B. White, G. J. Wasserburg, *Geol. Soc. Am. Bull.* **103**, 82 (1991).
11. C. D. Gallup, R. L. Edwards, R. G. Johnson, *Eos* **72**, 271 (1991).
12. B. Hamelin, E. Bard, A. Zindler, R. G. Fairbanks, *Earth Planet. Sci. Lett.* **106**, 169 (1991).
13. J. L. Banner, G. J. Wasserburg, J. H. Chen, J. D. Humphrey, *ibid.* **107**, 129 (1991).
14. E. Bard, R. G. Fairbanks, B. Hamelin, A. Zindler, C. T. Hoang, *Geochim. Cosmochim. Acta* **55**, 2385 (1991).
15. A. N. Dia, A. S. Cohen, R. K. O'Nions, N. J. Shackleton, *Nature* **356**, 786 (1992).
16. T.-L. Ku, K. G. Knauss, G. G. Mathieu, *Deep-Sea Res.* **24**, 1005 (1977).
17. F. M. Richter and K. K. Turekian, *Earth Planet. Sci. Lett.* **119**, 121 (1993).
18. T.-L. Ku, M. Ivanovich, S. Luo, *Quat. Res.* **33**, 129 (1990).
19. M. Stein *et al.*, *Geochim. Cosmochim. Acta* **57**, 2541 (1993).
20. G. M. Henderson, A. S. Cohen, R. K. O'Nions, *Earth Planet. Sci. Lett.* **115**, 65 (1993).
21. The isotopic composition of coral that gains extraneous ^{234}U and ^{230}Th at constant rates is

$$\delta^{234}U = \frac{R_{234}(1000)}{\lambda_{238}N_{238}}\left(1 - e^{-\lambda_{234}T}\right) + \delta^{234}U_i\, e^{-\lambda_{234}T} \quad (1)$$

$$\left[\frac{^{230}Th}{^{238}U}\right] = \frac{\lambda_{230}}{\lambda_{230} - \lambda_{234}}\left[\frac{\delta^{234}U_i}{1000} - \frac{R_{234}}{\lambda_{238}N_{238}}\right]\left(e^{-\lambda_{234}T} - e^{-\lambda_{230}T}\right) - e^{-\lambda_{230}T}\left(\frac{R_{234} + R_{230}}{\lambda_{238}N_{238}} + 1\right) + \frac{R_{234} + R_{230}}{\lambda_{238}N_{238}} + 1 \quad (2)$$

where [^{230}Th/^{238}U] is the ^{230}Th/^{238}U activity ratio, T is the true age, R_{234} and R_{230} are the rates of ^{234}U and ^{230}Th addition in atoms per unit mass of coral per unit time, and λ's are the decay constants [see (*4, 5*)]. The derivation of Eqs. 1 and 2 is analogous to that for δ^{234}U and [^{230}Th/^{238}U] (as a function of time) for a closed system, as in (*5*),

except that one solves differential equations with the additional constants R_{230} and R_{234}

$$\frac{dN_{230}}{dT} = \lambda_{234}N_{234} - \lambda_{230}N_{230} + R_{230} \quad (3)$$

$$\frac{dN_{234}}{dT} = \lambda_{238}N_{238} - \lambda_{234}N_{234} + R_{234} \quad (4)$$

where T is time and N refers to the number of atoms per unit mass of the isotope indicated. Equations 1 and 2 were determined by integration of Eqs. 3 and 4 with the initial condition that $^{230}Th/^{238}U = 0$ at $T = 0$. We solved for R_{234} and R_{230} with sample VA-1, using its measured isotopic composition (*4, 5*) (Fig. 2) for $\delta^{234}U$ and $[^{230}Th/^{238}U]$ and its uranium-helium age (T = 520 ka) [M. L. Bender *et al.*, *Geol. Soc. Am. Bull.* **90**, 577 (1979)] for T. We chose this sample because its isotopic composition is clearly the result of alteration, as it lies outside the range of isotopic compositions possible through closed-system evolution (*5*). For VA-1, R_{234} and R_{230} are 133,000 and 94,300 atoms per year per gram of coral, respectively. It is surprising that R_{234} and R_{230} are similar, given that uranium tends to be soluble and thorium insoluble in natural waters. In theory, redistribution of nuclides would rely on transport by ground water, yet the results of the model suggest the differential solubilities of uranium and thorium do not play a significant role in how they are transported and deposited. It may be that the nuclides are transported on particles in the water, such as organic colloids, which may be more likely to attract uranium and thorium in equal proportions [see J. K. Osmond and M. Ivanovich, in *Uranium-Series Disequilibrium: Applications to Earth, Marine, and Environmental Sciences*, M. Ivanovich and R. S. Harmon, Eds. (Clarendon, Oxford, 1992), pp. 259–289].

22. Deviations from a calculated trend may result from inaccuracies in model assumptions or from true differences in age between samples from a given terrace.
23. Sample UWI-2 crops out in the Rendezvous Hill Terrace, 33 m below its crest. The ^{230}Th age of 129.1 ± 0.8 ka indicates it grew at about the time of the last interglacial period. The sample is either (i) part of a slump, (ii) from a relatively low sea level between two possible last-interglacial sea-level highs (*19*), or (iii) from the sea-level rise immediately before the last interglacial period. To distinguish among these possibilities, similar deposits with clearer stratigraphic relationships must be studied.
24. The uplift rate is calculated by subtracting the estimated maximum eustatic sea level during the last interglacial, 2 to 8 m above present sea level (*10, 26*), from the present height of the last-interglacial terrace and dividing by the age. To calculate the original height of a given deposit, we determine the amount of uplift by multiplying its age by the uplift rate and subtracting the product from its present elevation. This calculation assumes constant uplift. Errors in calculated paleo–sea levels are based on a quadratic combination of errors in the initial height of the last-interglacial terrace [5 ± 3 m above present sea level (*26*)] and in the measured elevations of the samples. Sample WAN-D-3 is not in Table 2, but it also contains paleo–sea level information. It has a ^{230}Th age of 229.5 ± 4.3 ka with an initial $\delta^{234}U$ of 191 ± 4, a value outside the range of accuracy by our criterion. However, given the trend of the coral data in Fig. 2, WAN-D-3 is likely older than 200 ka. Using its present height and an age of 215 ± 15 ka to bracket its plausible age, we calculate an initial sea level of 28 ± 9 m below the present level. Thus, it seems likely that terrace WAN-D correlates with and constrains sea-level elevation for one of the stadials in oxygen isotope stage 7, possibly substage 7.2.
25. D. A. Richards, P. L. Smart, R. L. Edwards, *Eos* **73**, 172 (1992); *Nature*, in press.
26. T.-L. Ku, M. A. Kimmel, W. H. Easton, T. J. O'Neil, *Science* **183**, 959 (1974); J. F. Marshall and B. G. Thom, *Nature* **263**, 120 (1976).
27. E. Bard, B. Hamelin, R. G. Fairbanks, A. Zindler, *Nature* **345**, 405 (1990); E. Bard *et al.*, *Nuclear Instrum. Methods Phys. Rev. Sect. B* **52**, 461 (1990); E. Bard, M. Arnold, R. G. Fairbanks, B. Hamelin, *Radiocarbon* **35**, 191 (1993).
28. We have included Bahamian data in our analysis because the Bahamas have a climate similar to that of Barbados. We have not included data from Papua New Guinea (*15, 19*), which include nominal last-interglacial ages as old as 134 ka, or from Hateruma Atoll (*20*) because samples from these localities have initial $\delta^{234}U$ values both higher and lower than the modern value [(*15, 19, 20*); C. D. Gallup and R. L. Edwards, unpublished data] that lack consistent isotopic trends, suggesting more complex diagenetic processes than we have modeled. These complex processes may be a result of the high annual rainfall these areas receive.
29. Data for which the nominal initial $\delta^{234}U$ value is less than or equal to 158 meet our criterion.
30. W. S. Broecker and G. H. Denton, *Geochim. Cosmochim. Acta* **53**, 2465 (1989).
31. I. J. Winograd *et al.*, *Science* **258**, 255 (1992); K. R. Ludwig *et al.*, *ibid.*, p. 284.
32. The ice volume before a given high-sea-level event may be one of these factors, for example; W. R. Peltier and W. T. Hyde, *J. Atmos. Sci.* **44**, 1351 (1986).
33. J. Imbrie *et al.*, in *Milankovitch and Climate: Part 1*, A. Berger, J. Imbrie, G. Kukla, B. Saltzman, Eds. (Reidel, Dordrecht, Netherlands, 1984), pp. 269–306.
34. See A. Kaufman, *Quat. Res.* **25**, 55 (1986) for review; R. G. Johnson, *Geology* **19**, 686 (1991).
35. A. L. Bloom, W. S. Broecker, J. M. A. Chappell, R. K. Matthews, K. J. Mesolella, *Quat. Res.* **4**, 185 (1974).
36. R. L. Edwards and C. D. Gallup, *Science* **259**, 1626 (1993); K. R. Ludwig, K. R. Simmons, I. J. Winograd, B. J. Szabo, A. C. Riggs, *ibid.*, p. 1626; N. J. Shackleton, *Nature* **362**, 596 (1993); K. R. Ludwig *et al.*, *ibid.*, p. 596.
37. J. Imbrie, A. C. Mix, D. Martinson, *Nature* **363**, 531 (1993); R. G. Johnson and H. E. Wright Jr., *Science* **246**, 262 (1989); I. J. Winograd and T. B. Coplen, *ibid.*, p. 262.
38. J. D. Humphrey, *Sedimentology* **35**, 327 (1988).
39. A. Kaufman and W. S. Broecker, *J. Geophys. Res.* **70**, 4039 (1965).
40. R. G. Lighty, I. G. MacIntyre, R. Stuckenrath, *Nature* **276**, 59 (1978).

41. We thank M. Hinds for sharing her thorough knowledge of Barbados, D. Herbert for assistance in the field, M. K. Reagan, J. L. Banner, D. A. Richards, H. E. Wright Jr., J. W. Beck, K. R. Miller, and F. W. Taylor for insightful comments and discussions, the reviewers for helpful comments, and R. K. Matthews for sample AFM-20. Supported by National Geographic Society (4481-91 and 4887-92), the National Science Foundation (EAR-8904705, EAR-8904895, ATM-8921760, and EAR-8817260 for the TIMS facility), and the University of Minnesota.

2 July 1993; accepted 13 December 1993

Nanowire Array Composites

C. A. Huber,* T. E. Huber, M. Sadoqi, J. A. Lubin, S. Manalis, C. B. Prater

Long, nanometer-size metallic wires can be synthesized by injection of the conducting melt into nanochannel insulating plates. Large-area arrays of parallel wires 200 nanometers in diameter and 50 micrometers long with a packing density of 5×10^8 per square centimeter have been fabricated in this way. When charged, the ends of the wires generate strong, short-range electric fields. The nanowire electric fields have been imaged at high spatial resolution with a scanning force microscope.

The design of composite materials consisting of a mixture of various phases in the nanometer size range has flourished in the last few years (*1, 2*). The bulk electronic and optical properties of such nanocomposites can be tailored by altering the constituents, their size and shape distributions, or their relative concentrations. We describe a class of composites consisting of a high-density array of parallel, nanometer-size, metallic wires embedded in a dielectric matrix. The composite preparation makes use of porous insulators with a regular nanochannel structure as host or template. The small channels in the host are filled with the conducting phase by high-pressure injection of its melt (*3, 4*). In contrast to other microporous materials, such as the silica glasses of the Vycor type, which support a random network of pores, the regular nanochannel matrices allow for the preparation of nanocomposites whose physical properties are easier to interpret and

C. A. Huber, Research and Technology Department, Naval Surface Warfare Center, Silver Spring, MD 20903, USA.
T. E. Huber and M. Sadoqi, Department of Physics, Polytechnic University, Brooklyn, NY 11201, USA.
J. A. Lubin, Laser Chemistry, Howard University, Washington, DC 20059, USA.
S. Manalis and C. B. Prater, Digital Instruments, Santa Barbara, CA 93103, USA.
*To whom correspondence should be addressed.

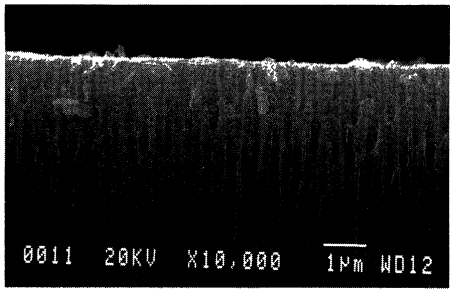

Fig. 1. Cross section of the top surface of an alumina with 200-nm nominal channel diameter, obtained by cleavage of the plate.